First-principles study of the electronic structure and the Fermi surface in rare-earth filled skutterudites $R\mathrm{Pt_4Ge_{12}}$

Gheorghe Lucian Pascut,[1,2] Michael Widom,[3] Kristjan Haule,[1] and Khandker F. Quader[4,*]
[1]*Department of Physics & Astronomy, Rutgers University, Piscataway, New Jersey 08854, USA*
[2]*MANSiD Research Center and Faculty of Forestry, Stefan Cel Mare University (USV), Suceava 720229, Romania*
[3]*Department of Physics, Carnegie Mellon University, Pittsburgh, Pennsylvania 15213, USA*
[4]*Department of Physics, Kent State University, Kent, Ohio 44242, USA*

(Received 30 April 2019; revised manuscript received 12 July 2019; published 5 September 2019)

Experiments on rare-earth filled skutterudites demonstrate an intriguing array of thermodynamic, transport, and superconducting properties, and bring to fore theoretical challenges posed by f-electron systems. First-principle calculations based density functional theory and its extensions for strongly correlated systems such as the Hubbard U correction, provide valuable information about electronic structure that can be used to understand experiments. We present a comprehensive study of the electronic structure and Fermi surface of a series of rare-earth filled skutterudites, $R\mathrm{Pt_4Ge_{12}}$ (where R = La, Ce, Pr), aimed at shedding light on: consequences of progressive increase of f-orbital occupancy in the series; the effects of the Hubbard parameter U; and the Fermi surfaces, band structures, and densities of states. The calculated Fermi surfaces may be relevant to the question of multiband versus single-band superconductivity. Computed densities of states qualitatively explain the available resonant photoemission spectroscopy experiments, and (together with available specific heat measurements) provide estimates of the effective masses. We also show the existence of pseudogaps in the total density of states which may be relevant for the thermoelectric properties of these systems.

DOI: 10.1103/PhysRevB.100.125114

I. INTRODUCTION

Filled skutterudites are a class of materials that exhibit complex crystal structures [1,2], and correspondingly complex electronic ground states, such as conventional BCS type [3] and unconventional superconductivity [4–6], non-Fermi liquid behavior [7,8], anomalous metal-to-insulator transition [9], multipolar ordering [10], topological insulator state [11,12], Kondo lattice behavior [3], valence fluctuations [13], heavy fermion behavior [14–16], various magnetically ordered states [17–20], etc. They are also promising materials for next generation thermoelectric applications [21–24].

In this paper, using first-principles density functional theory (DFT) and its extensions for strongly correlated systems, we address open questions about the Fermi surface topology and its s, p, d, and f character in the recently synthesized $R\mathrm{Pt_4Ge_{12}}$ filled skutterudites with R = La, Ce, or Pr. Our study is driven by the large body of experimental work on the $R\mathrm{Pt_4Ge_{12}}$ that demonstrate an array of novel properties [3,6,7,9,17,21]. Existing experimental results (summarized in Sec. II) point to the need for a comparative study of electronic properties in $R\mathrm{Pt_4Ge_{12}}$ compounds. Such a study would be useful to understand similarities and differences between these materials and the consequence of these for macroscopic properties. Despite some existing density of states (DOS) calculations [25–28], a comprehensive study across the range of these compounds including spin-orbit coupling (SOC) and the Hubbard parameter U is still lacking. As pointed out in Ref. [29], such calculations may shed light on the possible multiband nature of superconductivity and the origin of multiple and/or complicated pairing mechanisms. Thus our paper reports a systematic and comparative study of the $R\mathrm{Pt_4Ge_{12}}$ electronic structure.

The complex crystal structure of the filled skutterudites [shown in Fig. 1(a)] is stabilized by adding an electropositive ion to the empty voids of the skutterudites [see Fig. 1(b)]. Besides stabilizing the crystal structure, it turns out that the electropositive ion (which in our work is La, Ce, or Pr) also gives rise to novel electronic states [2] and improved thermoelectric properties [24]. Considering the complex crystal structure and the fact that usually f-electron systems pose challenges for DFT methods [30,31], we confirm the robustness of our main results by carrying out an extensive study under various theoretical scenarios such as DFT + SOC and DFT + SOC + U with the f electrons treated as core or valence electrons. Among our goals is to understand the changes in the electronic structure and Fermi surface (FS) topology and its character, as we progress from La to Ce and Pr, possessing, respectively, 0, 1, and 2 f electrons in their pure elemental states.

We find that independently of the theoretical approximation used in our calculations: (I) multiple large Fermi surfaces exists in $R\mathrm{Pt_4Ge_{12}}$, a feature similar to that in $\mathrm{MgB_2}$ where multiband superconductivity is found [32,33]. (II) The large FS have anisotropic orbital character on the FS, a feature similar to the FS in Pb where multiband superconductivity is also found [34,35]. (III) In all $R\mathrm{Pt_4Ge_{12}}$ compounds the states at E_F are dominated by Ge-p states. (IV) f states are always present at E_F for $\mathrm{CePt_4Ge_{12}}$ and $\mathrm{PrPt_4Ge_{12}}$ independently of the values of the Hubbard parameter U. (V) SOC lifts band degeneracy, shifts bands, and affects the topology of the

*quader@kent.edu

 ©2019 American Physical Society

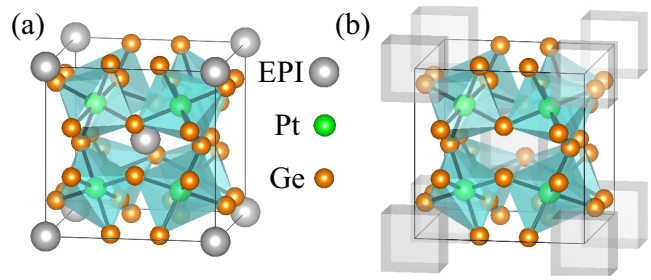

FIG. 1. Crystal structure: (a) filled skutterudite and (b) skutterudite. EPI stands for electropositive ion. The voids, mentioned in the text, are shown by the cubic transparent shapes.

Fermi surfaces. (VI) DOS show deep pseudogaps above E_F which may have implications for thermoelectric properties. In addition, our DFT + SOC + U calculations qualitatively explain features observed in photoemission experiments, while revealing a need for improved treatment of the f-electrons systems. We also find that the deduced values of the mass enhancement are not insignificant signaling the existence of modest correlations in these materials.

The paper is organized as follows. In Sec. II we give a brief overview of the experimental behavior of filled skutterudites. Section III is devoted to a discussion of the methods used for our calculations and the different theoretical scenarios considered. This is followed by Sec. IV where we present the results for the rare-earth filled skutterudites, $R\mathrm{Pt_4Ge_{12}}$ (R = La, Ce, Pr) under different scenarios, namely PBE, PBE + SOC, PBE + SOC + U. Results for band structure, energy bands, and FS without the the inclusion of Hubbard-like correlation U are presented in Secs. IV A, IV B, and IV C, respectively, and the effects of including U on DOS and FS are presented in Sec. IV D. In Sec. IV E, based on measurements of low-temperature specific heat, we provide simple estimates of the effective mass enhancements over the calculated density of state mass m^*/m_s for the various theoretical scenarios considered. We mention possible thermoelectric application of the $R\mathrm{Pt_4Ge_{12}}$ in Sec. V. We end the main text with discussions in Sec. V and acknowledgments. We note that we provide additional details in the Appendixes.

II. EXPERIMENTAL BACKGROUND

Experiments on $\mathrm{BaPt_4Ge_{12}}$, $\mathrm{SrPt_4Ge_{12}}$, and $R\mathrm{Pt_4Ge_{12}}$ skutterudites reveal a diverse array of interesting properties: while Ba-, Sr-, La-, $\mathrm{PrPt_4Ge_{12}}$ exhibit superconductivity at 5.1, 5.35, 8.3, and 7.9 K, respectively [25,36,37], $\mathrm{CePt_4Ge_{12}}$ does not show superconductivity, and instead it is believed to demonstrate a mixed valence or Kondo lattice behavior, or possibly a behavior in between [13,26]. $\mathrm{NdPt_4Ge_{12}}$ and $\mathrm{EuPt_4Ge_{12}}$ are characterized by antiferromagnetic transitions at 0.67 and 1.7 K, respectively [25]. $\mathrm{SmPt_4Ge_{12}}$ exhibits [38] heavy fermion behavior with a large value of the electronic specific heat coefficient ($\gamma \sim 450/\mathrm{mol/K^2}$), indicating the possibility of strong correlations in this material.

In the Ba, Sr, and La compounds, experiments point to conventional nodeless s-wave BCS pairing; however, sublinear behavior of the field-dependent electronic part of specific heat $C_V(H)$ and thermal conductivity $\kappa(H)$ may indicate two equal-sized s-wave superconducting gaps in $\mathrm{LaPt_4Ge_{12}}$ [28,39,40]. The nature of pairing in $\mathrm{PrPt_4Ge_{12}}$ is less settled. Low-T specific heat and muon spin resonance measurements claim evidence for unconventional pairing with point nodes in the gap [5]. But, several other experiments point to multiband superconductivity with two superconducting gaps. Lower and upper critical field measurements and photoemission spectroscopy (PES) [41,42], and upturn in the temperature dependence of the upper critical field [28,40,43], indicate multiband paring. Strong indication of two-gap superconductivity (as in $\mathrm{MgB_2}$ [32,33,44,45] and Pb [34,35,46]) has been found in the analysis of superfluid density in *single* crystal $\mathrm{PrPt_4Ge_{12}}$ [29], the only single crystal measurement in this material that we are aware of. Multiband pairing with one nodeless and one nodal gap has been inferred [47] from fitting low-T specific heat data in $\mathrm{PrPt_4Ge_{12}}$ and $\mathrm{Pr_{1-x}Ce_xPt_4Ge_{12}}$, while other work based on transport and thermodynamic measurements on $\mathrm{Pr_{1-x}Ce_xPt_4Ge_{12}}$ [48] and $\mathrm{PrPt_4Ge_{12-x}Sb_x}$ [19] leave open the possibility of nodal versus multiband superconductivity. ^{73}Ge nuclear quadrupole resonance [49] shows a coherence peak below pairing transition temperature, typical of BCS pairing.

A detailed study of the electronic structure of $R\mathrm{Pt_4Ge_{12}}$ may be able to shed some light on the extent to which the Pr $4f$ electrons play a role in these couplings, and thereby indirectly playing a role in multiband pairing and gaps. The strong experimental indication of multiband pairing in $\mathrm{PrPt_4Ge_{12}}$, and possibly in $\mathrm{LaPt_4Ge_{12}}$, is suggestive of a complex band structure with several bands crossing the Fermi surface. Therefore a detailed study of the electronic properties in $R\mathrm{Pt_4Ge_{12}}$ is necessary.

The $R\mathrm{Pt_4Ge_{12}}$ materials studied here do not exhibit long range magnetic order. $\mathrm{LaPt_4Ge_{12}}$ is diamagnetic at all temperatures, while the f electrons in $\mathrm{CePt_4Ge_{12}}$ and $\mathrm{PrPt_4Ge_{12}}$ obey Curie-Weiss behavior at sufficiently high temperatures. For $\mathrm{PrPt_4Ge_{12}}$, the magnetic susceptibility starts to exhibit a Curie-Weiss behavior for $T > 100$ K [13] with experimental average effective magnetic moment μ_{CW} of 3.59 [13] or 3.69 μ_B/f.u. [25,48] (μ_B being Bohr magneton) that are close to that of the free $\mathrm{Pr^{3+}}$ ion (3.58 μ_B) with the electronic configuration $4f^2$ and the $^3H_4$ Hund rule ground state multiplet, indicating the presence of local moments on the Pr ions. However, the magnetic susceptibility saturates at low temperatures, indicating a nonmagnetic ground state, a scenario that is consistent with the crystal field splitting of the degenerate $^3H_4$ Hund rule ground state multiplet [13,25].

In the case of $\mathrm{CePt_4Ge_{12}}$, the magnetic susceptibility has also a Curie-Weiss behavior down to 200 K [13] with experimental average effective magnetic moment μ_{CW} of 2.58 or 2.51 μ_B/f.u. [26] that are close to that of the free $\mathrm{Ce^{3+}}$ ion (2.54 μ_B) with the electronic configuration $4f^1$ and the $^2F_{5/2}$ Hund rule ground state multiplet, indicating the presence of local moments on the Ce ions. Below 200 K, the susceptibility deviates from Curie-Weiss and exhibits a broad maximum at 80 K, followed by an upturn below ~20 K [13,26]. The broad maximum can be interpreted as a characteristic feature of intermediate valence [13] or as indicative of local moment screening with a large characteristic energy [26].

From all $R\mathrm{Pt_4Ge_{12}}$ compounds studied here, $\mathrm{CePt_4Ge_{12}}$ is the only one where a long range order, of antiferromagnetic

type, can be stabilized at low temperatures upon Sb substitution of Ge [50]. Due to the absence of local moments in $LaPt_4Ge_{12}$ or the nonmagnetic ground state of the Pr ions in $PrPt_4Ge_{12}$, no long range magnetic order is found in $LaPt_4Ge_{12}$ or $PrPt_4Ge_{12}$ compounds.

In addition to superconducting, magnetic, and transport properties, filled skutterudites appear promising with respect to their thermoelectric capabilities [51]. Since the capabilities of a thermoelectric material is a consequence of the interplay between the transport quantities such as the Seebeck coefficient S, the electrical resistivity ρ, and the thermal conductivity κ, optimizing these quantities in a material could give rise to a large thermoelectric figure of merit $ZT \geqslant 1$, that is required for reasonable performance of a thermoelectric material. Recently it was shown that ZT could be further improved in filled skutterudites by tuning the thermal conductivity based on the so-called phonon glass and electron crystal (PGEC) concept which was developed for cage-forming structures in general [52–54]. In addition, related to the materials studied in this work, it has been shown that by substituting Ge by Sb in $LaPt_4Ge_{12}$ compound, the Seebeck coefficient and resistivity could be enhanced by an order of magnitude at room temperature [51], thus increasing the playground to optimize the figure of merit ZT.

III. METHODS

All our calculations are based on the electronic density functional theory method [55,56] with the Perdew-Burke-Ernzerhof (PBE) generalized gradient approximation [57] to the exchange-correlation potential. Calculations are performed on the experimental crystal structures (measured atomic positions and lattice parameters [2], as shown in Tables II, III, and IV in Appendix D) having the Im-3 cubic space group [2].

For each compound, we studied in detail the electronic band structure, DOS, and FS under various theoretical scenarios such as PBE, PBE + SOC, and PBE + SOC + U. For each of these scenarios the rare-earth f electrons were treated either as valence electrons or core electrons. We include SOC and U in our calculations due to the fact that they are important energy scales for rare-earth elements.

As discussed in Sec. II, experiments show that the RPt_4Ge_{12} compounds studied here (in particular, the Ce and Pr skutterudites) are Fermi liquids with no magnetism. It is also well known that DFT calculations can produce multiple solutions, depending on the specific DFT scenario, directions of initial magnetic moments, etc. In examining the manifold of solutions, we find that our spin-polarized solutions within PBE + SOC and PBE + SOC + U have slightly lower energy compared to the non-spin-polarized ones (elaborated upon below), but the magnetic moments (spin and orbital) are very small. Based on this, one could either adopt the solutions obtained by constraining the net moment to be zero (to be consistent with experiments) or take the slightly lower energy solutions with very small moments, *albeit* not consistent with experiments. We have chosen to report results of the first scenario to be consistent with experiments. Our results, such as Fermi surfaces, density of states, and spectral functions, can then be viewed as predictions to be tested against further experiments. For ordinary PBE calculations we obtain these by working with non-spin-polarized calculations. For PBE + SOC in VASP we initialize the moments to zero and this is preserved under iteration to self-consistency. In WIEN2K, to obtain a non-spin-polarized solution within the PBE + SOC and PBE + SOC + U approximations, we first initialize the input files as we would do for a magnetic calculation. Then while performing the self-consistent calculations, we put the constraint that the total spin moment per unit cell be zero. The solution obtained with this procedure had all the spin moments zero (by spin moment we mean the spin moment inside the muffin-tin sphere around the atoms and the interstitial spin moment, thus obtaining a solution with zero spin magnetic moment per unit cell). In addition, we also find that we could obtain the same non-spin-polarized solution even if we first do a self-consistent magnetic calculation without any constraint, and then (starting from this spin-polarized solution), apply the constraint that the total spin moment per unit cell be zero. Additionally, we find that if we put the constraint on the spin moment, the orbital moments also come out to be zero.

In this work we combine results from VASP and WIEN2K codes, to take advantage of their strengths. We note that WIEN2K is an all electron code (core + valence electrons), while VASP works only with the valence electrons (while the potential of the atom nuclei and the core electrons is replaced by an effective potential known as a pseudopotential). Even though the basis sets in the two codes differ, as long as the basis set in each code is an almost complete basis, the results obtained by the two codes should be very similar. We compared the electronic band structure of the RPt_4Ge_{12} obtained by the two codes for each theoretical scenario used in this work and in each case we found very similar electronic structure, as expected.

Below, we give specific parameters used for the calculations in each code.

VASP. Electronic band structure and DOS calculations utilize the plane-wave based DFT code VASP [58] with the all-electron projector augmented wave (PAW) method [59]. We take the standard VASP PAW potentials, keeping the f orbitals as valence states (except where we specify f in the core). In addition, the Ge $3d$ orbitals are kept in the core. Increasing plane-wave energy cutoffs had no discernible impact on the band structure so we apply the VASP defaults. However, we use the full FFT grids consistent with the energy cutoff to represent charge densities so as to avoid wrap-around errors. Electronic k-point meshes are increased to $31 \times 31 \times 31$ in order to converge the electronic DOS, which we evaluate using tetrahedron integration followed by 0.01 eV Gaussian smearing.

WIEN2k. FS and the associated electronic band structure were performed using the full-potential linearized augmented plane-wave (FP-LAPW) method as implemented in the WIEN2K code [60]. The calculations were performed on a $31 \times 31 \times 31$ k-point mesh. The muffin-tin radii were chosen as 2.50, 2.45, and 2.22 bohr units for the rare-earth ions Pt and Ge, respectively. In order to have accurate calculations we used $R_{mt}K_{max} = 8$. The energy which separates the core and the valence states was chosen to be -10 Ry (for this energy cutoff, the Ge $3d$ orbitals are kept in core). Self-consistency criteria for the convergence of total energy and convergence of charge distance (as defined in WIEN2K), were 10^{-4} Ry and

10^{-4} electrons, respectively. All other input parameters were used with their default values.

IV. RESULTS

A. Overview of band structure

Figure 2 presents electronic band structure and atom-projected DOS for PBE and PBE + SOC approximations, where f electrons are treated as valence electrons. For each band structure plot, the k-point path that connects special **k** points in the first Brillouin zone (BZ) is defined as in Ref. [61]: Γ (0, 0, 0), H (1/2, −1/2, 1/2), N (0, 0, 1/2), and P (1/4, 1/4, 1/4).

Several things may be noted in the set of plots in Fig. 2.

(I) From the electronic band structure plots for the RPt$_4$Ge$_{12}$ compounds for a given approximation (rows in Fig. 2), we see that by going from La to Pr (which is equivalent with increasing the number of f electrons n_f from 0 to 2) new bands appear above the Fermi level (E_F) in the energy range 0.2–0.6 eV. The new bands are related to the Ce and Pr f electrons, and although they hybridize with the other bands in the system, we see that the bands in the vicinity of the E_F do not change their shape drastically in CePt$_4$Ge$_{12}$ and PrPt$_4$Ge$_{12}$ when compared to LaPt$_4$Ge$_{12}$, but they are shifted down in energy with respect to the E_F. Since the intersections of the bands with the E_F defines points on the 3D FS, shifting of the bands around the E_F will change the topology of the FS. Thus, we expect that the topology and the number of the FS in CePt$_4$Ge$_{12}$ and PrPt$_4$Ge$_{12}$ to be different from the FS in LaPt$_4$Ge$_{12}$.

(II) The atom-projected DOS gives information about the contribution/weight of each atom to the electronic band structure at a given energy. Thus our calculations show that in the La compound, the states at the E_F come mostly from the Pt and Ge atomic states and there are few or no La states. By contrast, in the Ce and Pr compounds, besides the Pt and Ge atomic states, we also have states from the rare-earth elements. As we will discuss later in paper this can have implications for the single versus multiband superconductivity in RPt$_4$Ge$_{12}$ compounds.

(III) Comparing plots with and without SOC for a given compound, see Figs. 2(a)–2(c) versus Figs. 2(d)–2(f), we see that SOC lifts the band degeneracy at special points and along various k paths in the first BZ and shifts some of the bands by up to a few hundred meV. For example, these effects are especially evident at the Γ and H points and along the Γ–P path. Since SOC has an impact on the electronic band structure, it also has a direct effect on the topology and degeneracy of the FS.

It is well known that for rare-earth elements, the occupied f states can behave as inert localized states in some compounds (and in those cases the f electrons must be treated as core in the theoretical approximations) or the f states can hybridize with the other states in the system (and in those cases the f electrons must be treated as valence electrons). In Appendix A we show the electronic band structure and atom-projected DOS, for the case where the f electrons are treated as core, thereby eliminating hybridization with the other states in the system. From the calculations with f electrons in the core, we learn that for a given approximation, these compounds have almost identical electronic band structure and thus almost the same FS as expected (see rows in Fig. 6). Thus, the theoretical approximations where the f electrons are treated as core electrons cannot explain the differences between the

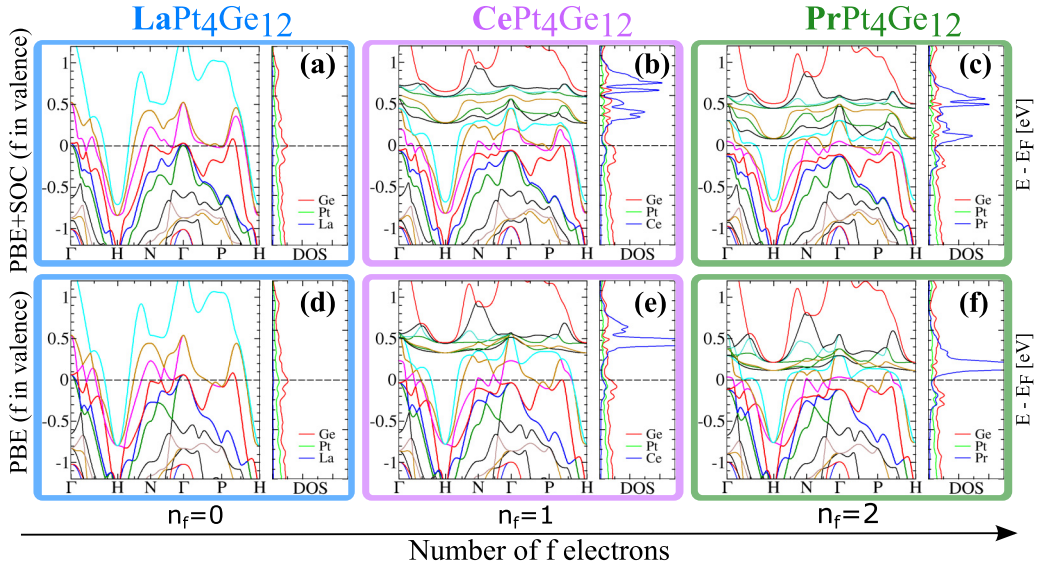

FIG. 2. Electronic band structure and atom-projected DOS results for RPt$_4$Ge$_{12}$ compounds obtained using the VASP code. Each column corresponds to a particular compound whose chemical formula is printed at the top of the column. Each row corresponds to results from calculations using a particular approximation whose label is printed at the beginning of the row. On the left side of each panel we show the electronic band structure (energy in eV on the vertical axis versus momentum on the horizontal axis). Fermi energy is marked by the horizontal dashed line. On the right side of each panel we show atom-projected DOS (each unit on the DOS axis represents 1 state/eV/f.u.).

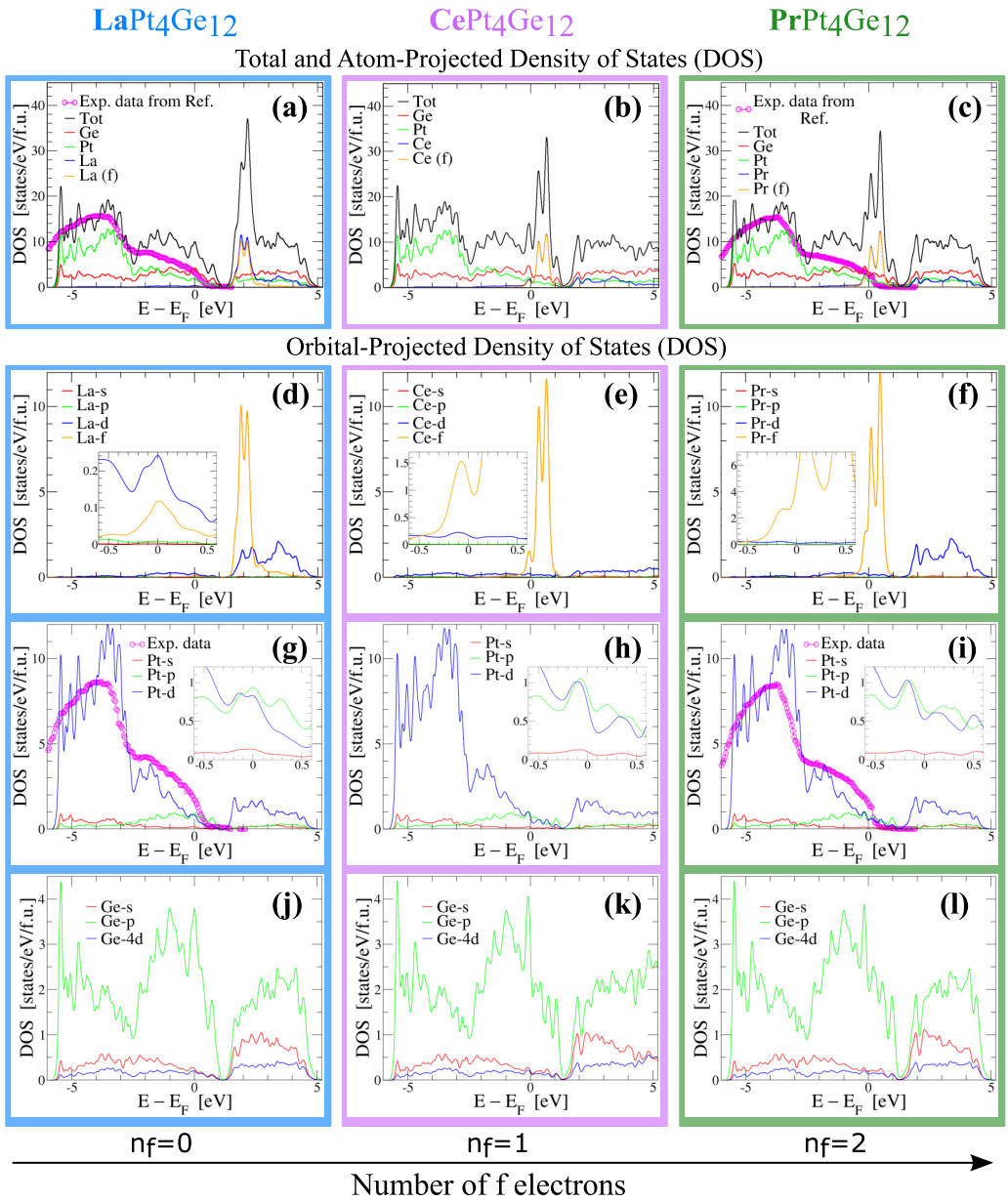

FIG. 3. Total, atom-, and orbital-projected DOS results for $R\mathrm{Pt}_4\mathrm{Ge}_{12}$ compounds. The results presented in this figure were obtained using the VASP code within the PBE + SOC constrained nonmagnetic approximation, treating the f electrons as valence electrons. Each column corresponds to a particular compound. Each panel on the first row corresponds to total, atom-, and f-projected DOS. Panels on the other three rows show orbital-projected DOS for the three distinct atoms making up these compounds. Fermi energy is marked by the zero on the horizontal axis. Some panels enlarge the DOS near the Fermi energy in an inset. The experimental soft x-ray photoemission spectra (measured with an incident energy of 1.2 keV) for $\mathrm{LaPt}_4\mathrm{Ge}_{12}$ and $\mathrm{PrPt}_4\mathrm{Ge}_{12}$ presented in Ref. [41] were digitized and included in our figures for comparison.

$\mathrm{LaPt}_4\mathrm{Ge}_{12}$ and $\mathrm{CePt}_4\mathrm{Ge}_{12}$ or $\mathrm{PrPt}_4\mathrm{Ge}_{12}$ compounds. The effects of SOC on the band structure are similar, independently of the way we treat the f electrons (in valence or in core).

B. Projected DOS

In Figs. 3(a)–3(c) we show the total DOS per formula unit of $R\mathrm{Pt}_4\mathrm{Ge}_{12}$ compounds together with the atom-projected DOS. In addition, in Figs. 3(d)–3(l) we also show the orbital-projected DOS for each atom within the $R\mathrm{Pt}_4\mathrm{Ge}_{12}$ compounds. These calculations were done using the PBE + SOC approximation within VASP with the f electrons treated as valence electrons. In this figure we also show the comparison of our calculations with the available experimental soft x-ray photoemission spectra [41]. We digitized the experimental data and we plot it on top of our calculated DOS in Figs. 3(a) and 3(c). Since the experimental data is in arbitrary units, we scaled it such that we get the best agreement between the experiment and theory in the energy range around −4 eV. We see that when comparing the experimental data with the total DOS per formula unit, by construction we get a good agreement for

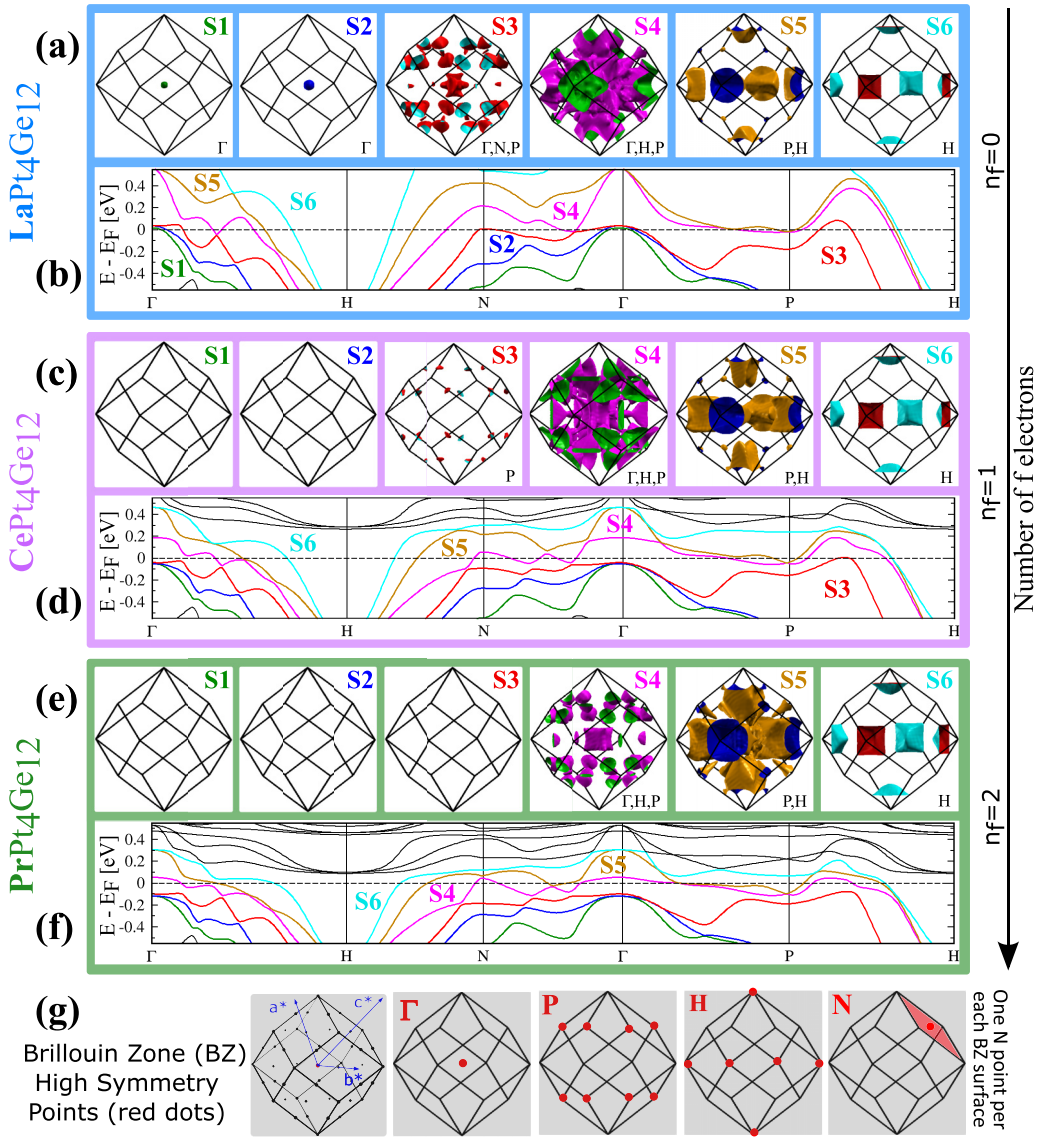

FIG. 4. Fermi surfaces (FS) for $R\mathrm{Pt}_4\mathrm{Ge}_{12}$ compounds obtained by using the WIEN2K code with the PBE + SOC constrained nonmagnetic approximation and treating the f electrons as valence electrons. Each diagram corresponding to one of the three compounds contains multiple panels showing the FS within the first Brillouin zone [(a), (c), and (e)] and the electronic band structure around the E_F](b), (d), and (f)]. FS and the corresponding bands have the same colors as the symbols Sn ($n = 1$ to 6) that represents them. (g) The reciprocal lattice vectors a^*, b^*, c^* and the position within first Brillouin zone (BZ) of the special reciprocal points Γ, P, H, N. On each FS panel, we also print the label of the special reciprocal points where the FS exists.

the energy range around −4 eV, but the agreement is poor for energy closer to the E_F. The reason for this discrepancy is the fact that the photoemission spectra were measured at an incident energy of 1.2 keV, energy where mostly Pt d states were probed, the other states practically being invisible to this probe due to the very small scattering cross section at this energy [41]. These discrepancies are expected since the total DOS per formula unit is a sum of all states with equal probability without considering the experimental scattering cross sections. But if we consider the scattering cross sections, and we compare the photoemission spectra only with the Pt d DOS as shown in Figs. 3(g) and 3(i), we see that the agreement between experiment and theory is much better over the full energy range.

Looking at all orbital projected DOS, see Figs. 3(d)–3(l), we see that the orbital contributions of the s, p, and d states at the E_F is similar for all three compounds. The difference is that in the case of Ce and Pr compounds, f states are also present at the E_F. This suggests that the electrons forming the Cooper pairs in $\mathrm{PrPt}_4\mathrm{Ge}_{12}$ might have some additional f character besides the s, p, and d, while in $\mathrm{LaPt}_4\mathrm{Ge}_{12}$ their character is mostly s, p, and d. Based on our results, and making an analogy with the case of Pb [34], where the anisotropic contributions of the s, p, and d orbital character to the wave functions forming the states at the E_F leads to anisotropic electron-phonon coupling and multiband superconductivity, we suggest the possibility of multiband superconductivity for $\mathrm{PrPt}_4\mathrm{Ge}_{12}$ and single- or multiband superconductivity for

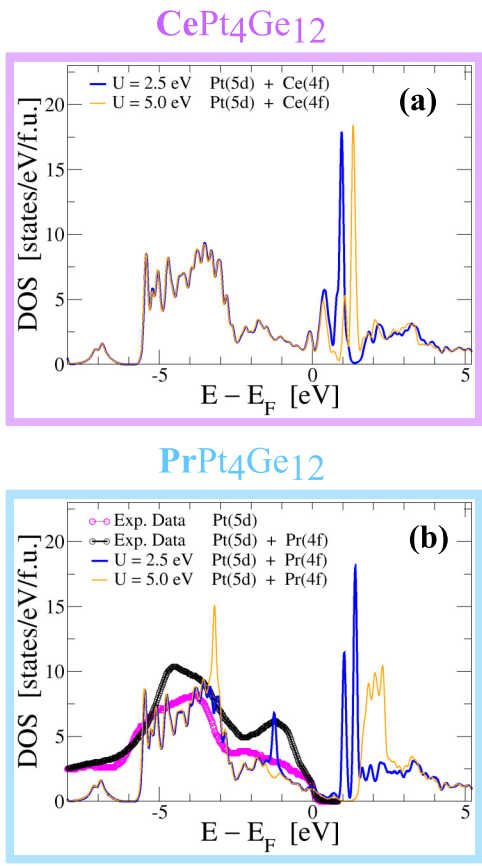

FIG. 5. Correlation effects on DOS. (a) and (b) Results of the PBE + SOC + U constrained nonmagnetic approximation for Ce and Pr compounds. The experimental soft x-ray photoemission spectra (measured with an incident energy of 1.2 keV magenta curve and 0.9 keV black curve) for $PrPt_4Ge_{12}$ presented in Ref. [41] were digitized and included in our figure for comparison. In addition, (b) shows the experimental spectra which has contributions mostly from Pt 5d states (magenta symbols) and the experimental spectra which has contributions from both Pt 5d and Pr 4f states (black symbols). For details see Fig. 2 in Ref. [41].

$LaPt_4Ge_{12}$. The pseudogaps found in the total DOS of the RPt_4Ge_{12} compounds might be relevant to possible improvement of their *thermoelectric effects*, as we will discuss later on in the paper.

C. 3D Fermi surfaces

Following up on our discussion on nonmagnetic solutions in Sec. III, we note that for the Fermi surfaces, there will not be much difference using the slightly lower energy spin-polarized solution or the non-spin-polarized solutions. So we choose to report the Fermi surfaces for the non-spin-polarized case, which are doubly degenerate, in comparison with the nearly degenerate Fermi surfaces in the spin-polarized case. In Fig. 4 we show the 3D FS (labeled by symbols Sn, $n = 1$ to 6) for the RPt_4Ge_{12}. These FS are calculated in WIEN2K, using the PBE + SOC approximation and treating the f electrons as valence electrons. In addition to the FS, we also show the electronic band structure for each compound in a narrow energy range around the Fermi energy.

As can be seen in Fig. 4(a), $LaPt_4Ge_{12}$ has six FS. The hole or electron pocket character can be ascribed to these FS by considering the corresponding band structure in Fig. 4(b). S1, S2, and S3 are hole pockets, and S5 and S6 are electron pockets. The character of S4 is not as clear from the band structure, see Fig. 4(b). Thus it is interesting to examine the changes of the FS with increasing number of f electrons. With 1 additional electron (compare Ce $4f^1$ with La $4f^0$), the Fermi energy increases, and the S1 and S2 hole pockets get filled while the S3 pocket is nearly filled, see Fig. 4(c). With the addition of another electron (the case of Pr $4f^2$) the S3 Fermi hole pocket is completely filled, see Fig. 4(e). The upshot is that $CePt_4Ge_{12}$ has four FS and $PrPt_4Ge_{12}$ has only three, see Figs. 4(c) and 4(e). Within the PBE + SOC approximation, the three compounds have in common three large FS, namely S4, S5, and S6. As the number of f electrons increases, S4 shrinks in size and hence has dominant hole character, while S5 grows and S6 is hardly affected. The S1–S3 hole pockets present in $LaPt_4Ge_{12}$ and absent in $CePt_4Ge_{12}$ and $PrPt_4Ge_{12}$ within the PBE + SOC approximation, show up within the PBE + SOC + U approximation for both $CePt_4Ge_{12}$ and $PrPt_4Ge_{12}$ compounds.

The orbital character of the FS may influence the nature of superconductivity. It is claimed that Pb has two Fermi surfaces [34,35], one spherical and one more complex. Owing to the anisotropic orbital character of the wave functions (s, p, and d across the two FS), the electron-phonon coupling varies across the FS and between the two FS, thereby giving rise to multiband superconductivity. It may also be recalled that in MgB_2, multiband superconductivity is given by two FS, both with p character (one FS is p_z in character and the other is $p_{x,y}$ in character) [32,33,43–45]. If the mechanism for superconductivity in the La and Pr compound is also phonon mediated, since there are multiple sizable FS as in MgB_2, this implies the possibility of multiband superconductivity in RPt_4Ge_{12}, as pointed out by experiments. In addition, since the Pr compound is shown to have f character on the FS (as shown by DOS in Fig. 3), this could lead to different electron-phonon couplings across the FS, similar to the anisotropic electron-phonon coupling found in Pb. Thus, the electron-phonon couplings may be different in $PrPt_4Ge_{12}$ compared to that in the $LaPt_4Ge_{12}$ case, thereby resulting in differences in the type of pairing. In order to ascertain the anisotropic orbital character across the FS, besides looking at the orbital projected DOS which gives an average of the orbital contribution over the all k points in the BZ, we also looked at the "fat-band" representation [62] around the E_F which gives a detailed description of the orbital contribution at specific k points in the BZ. The fat-band plots are shown in Appendix B. From the fat-band representation, we find anisotropic orbital character to the 3D FS for all the orbital states coming from R, Pt, and Ge atoms.

D. Effects of correlations on DOS and FS

Photoemission measurements on $PrPt_4Ge_{12}$ where the incident energy is scanned through the f resonance of the Pr atoms, reveal the presence f states at E_F and below. For example, see Fig. 5(b) where we show the digitized data from Ref. [41] for two incident energies, 1.2 and 0.9 keV.

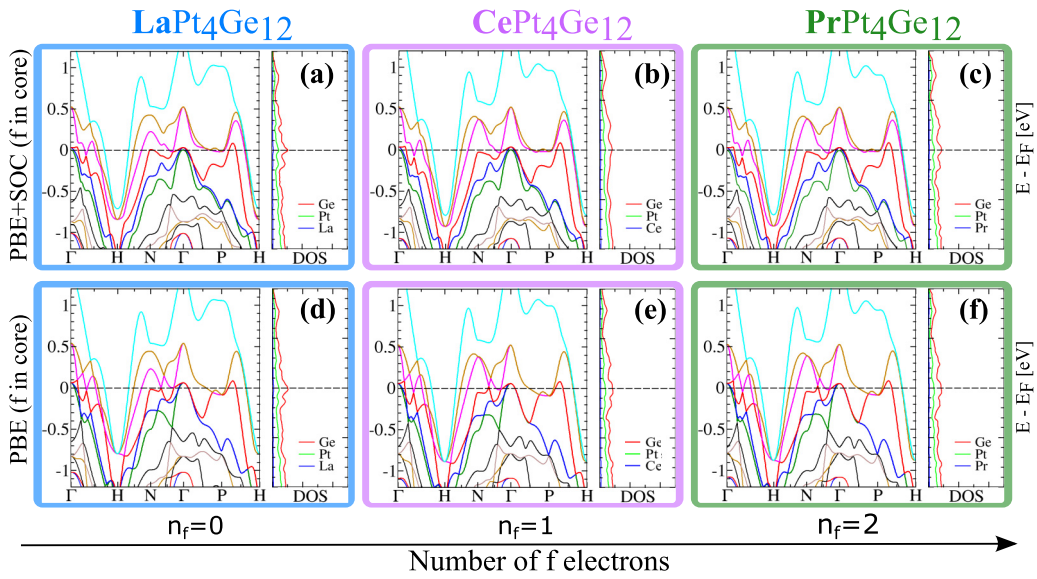

FIG. 6. Electronic band structure and atom-projected DOS results for $R\mathrm{Pt_4Ge_{12}}$ compounds obtained using the VASP code. These calculations were performed by placing the f electrons into core. Each column corresponds to a particular compounds whose chemical formula is printed at the top of the column. Each row corresponds to results from calculations using a particular approximation whose label is printed at the beginning of the row. Each panel presents results for a given compound within a given approximation. On the left side of each panel we show the electronic band structure (energy in eV on the vertical axis versus momentum on the horizontal axis). Fermi energy is marked by the horizontal dashed line. On the right side of each panel we show atom-projected DOS (each unit on the DOS axis represents 1 state/eV/f.u.).

For incident energy of 1.2 keV we probe mostly the Pt d states (magenta curve) and for incident energy of 0.9 keV, in addition to Pt d states, we also probe the Pr f states (black curve). Thus, the difference between the magenta and black curves in Fig. 5(b) represents the contribution of the Pr f states to DOS. Besides small contributions at the E_F, the Pr f states appear to manifest as two peaks centered around -1 and -4.5 eV which disagrees with our DOS calculations for the PBE + SOC approximation shown in Fig. 3(f). In order to explain the experimentally observed f contribution to DOS, shown in Fig. 5(b), we need to go beyond the DFT approximations. Repulsive interactions among the tightly bound f orbitals of the lanthanide atoms can create electronic correlations that are not properly modeled by our PBE

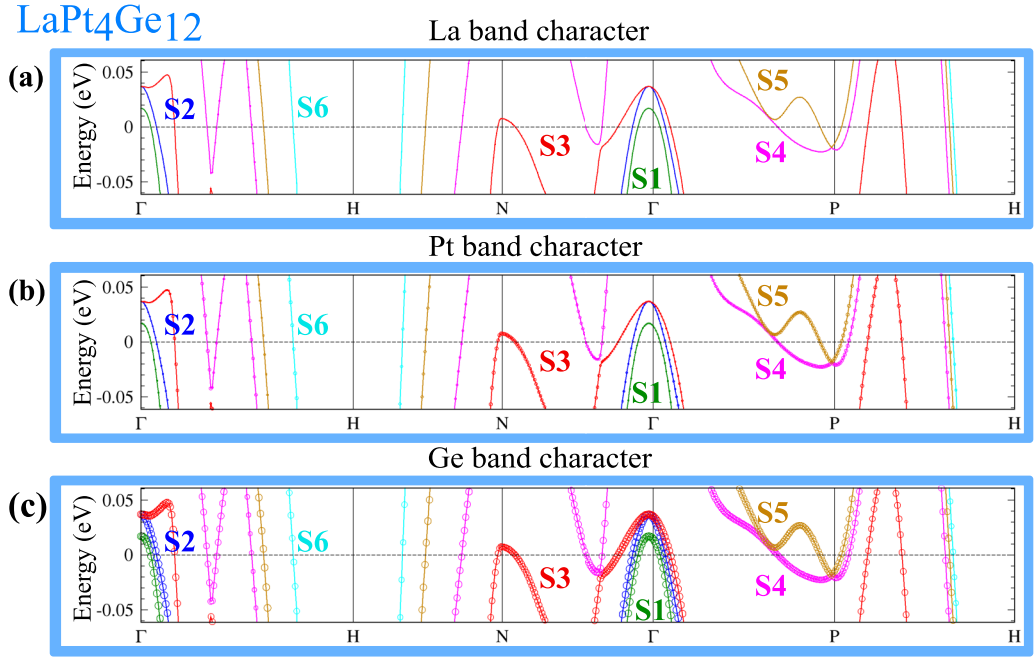

FIG. 7. Electronic band structure of $\mathrm{LaPt_4Ge_{12}}$ showing the atomic character of the bands. This figure enlarges the energy range near the Fermi energy of the band structure previously shown in Fig. 4. The sizes of the open circles at a given energy and momentum represent the wave function amplitude corresponding to a given atom as labeled in each panel.

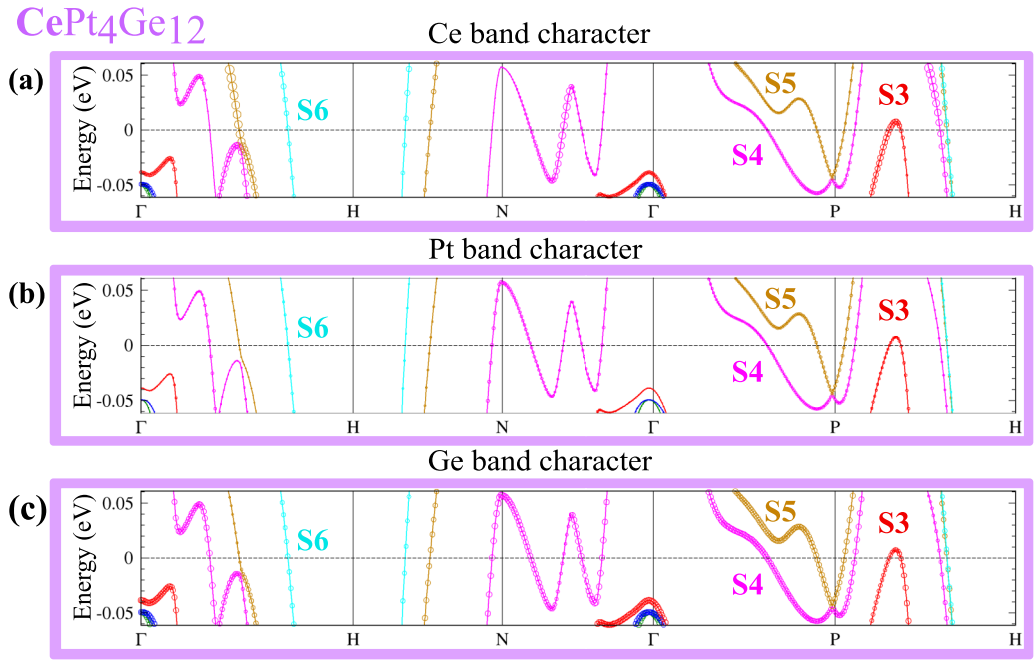

FIG. 8. Electronic band structure of $CePt_4Ge_{12}$ showing the atomic character of the bands. This figure enlarges the energy range near the Fermi energy of the band structure previously shown in Fig. 4. The sizes of the open circles at a given energy and momentum represent the wave function amplitude corresponding to a given atom as labeled in each panel.

density functional. A first step in correcting this effect is to supplement the DFT Hamiltonian with on-site Coulomb energies [63,64], which we take into account using a single effective Hubbard parameter U. We take $U = 5$ eV, a typical value for lanthanides, to illustrate the qualitative effect. For comparison, we also explore other values of U.

DOS computed within the PBE + SOC + U with $U = 0$ eV shown in Fig. 3 reveal that the f band is partly occupied, with the net f occupation of $n_f = 0.85$ for Ce and $n_f = 2.07$ for Pr. For $U > 0$, occupied and empty f orbitals split proportionately to U for Pr, but the splitting is far weaker for Ce, consistent with the respective values of n_f. For example, in Fig. 5 we show the Pt(d) + Ce(f) DOS for $CePt_4Ge_{12}$ and Pt(d) + Pr(f) DOS for $PrPt_4Ge_{12}$ compounds computed using $U = 2.5$ and 5.0 eV. As expected, the effect of U is to increase the splitting between the occupied and unoccupied f states, thus moving the theoretical f peak of occupied states in the Pt(d) + Pr(f) DOS, to lower energies. Comparing our theoretical DOS with the experimental data, we find that the position of the theoretical f DOS could explain the experimental peak shape at -1 eV for $U = 2.5$ eV or the peak at -4.5 eV for $U = 5.0$ eV, but our theory cannot explain both experimental peaks at the same time. This suggests that the PBE + SOC + U method captures part of the electronic correlation, but in order to explain the experimental findings a theory beyond DFT + U is required. One such theory, where correlation effects are treated more rigorously, is the density functional theory + embedded dynamical mean field theory (DFT + eDMFT) [65–67].

Since DOS at the E_F are affected by U, the FS of $CePt_4Ge_{12}$ and $PrPt_4Ge_{12}$ will also be affected. Since the positions of bands with respect to E_F directly relate to the topology of the FS, we also expect changes in the topology of the FS. While additional details are given in Appendix B (see Fig. 10 for $CePt_4Ge_{12}$ and Fig. 11 for $PrPt_4Ge_{12}$), we note a few salient points here. The band corresponding to the S6 FS does not change too much with increasing U indicating that it is mostly s, p, and d in character. The bands corresponding to S4 and S5 change with increasing U, S4 being more affected than S5, suggesting that these FS having stronger f character than S6. To confirm the contribution of f states to the S4 and S5 FS for finite U values, we have also computed the FS for the case where the f electrons are treated as core electrons (in this case the Fermi surface has no f contribution). The fact that the topology of the FS for finite U differs from the case where the f electrons are treated as core electrons (labeled $U \sim \infty$ eV in Appendix B Figs. 10 and 11), confirms once again the presence of f character in the Fermi surface of $CePt_4Ge_{12}$ and $PrPt_4Ge_{12}$, independently of the strength of correlations. In addition, we also learn that the presence or absence of the S1, S2, and S3 FS in $CePt_4Ge_{12}$ and $PrPt_4Ge_{12}$ depends on the strength of the correlations.

E. Effective mass

While our calculations show that the rare-earth filled skutterudites have complex band structures and DOS, simple estimates of effective mass can nevertheless be obtained by considering the linear coefficient of the specific heat obtained experimentally in these materials. The electronic specific heat $C_V(T)$ in metals, for $T \ll T_F$ (T_F being the Fermi temperature), is given by [68]

$$C_V = \gamma T = \tfrac{1}{3}\pi^2 k_B^2 N(E_F) T. \quad (1)$$

For a spherical FS with parabolic bands, the linear coefficient of specific heat γ is related to the electronic DOS at the E_F

TABLE I. Theoretical DOS at E_F and the corresponding estimated mass enhancement over the DOS mass m^*/m_s (see text for details). For a given compound, different m^*/m_s correspond to different measurements of γ, the linear coefficient of specific heat C_V, in units of mJ/mol K^2.

	$D(E_F)$ (states/eV/f.u.) calc.			m^*/m_s est.		
DFT scenarios	La	Ce	Pr	La[a,b]	Ce[c]	Pr[d,e,f]
PBE (f in valence)	11.9	10.9	14.7	2.7/2.0	4.1	2.5/2.1/2.0
PBE+SOC	10.0	12.2	16.4	3.2/2.4	3.7	2.3/1.9/1.8
PBE+SOC+$U(=5)$	–	10.0	11.3	–	4.5	3.3/2.8/2.6
PBE (f in core)	–	9.6	9.6	–	4.7	3.9/3.3/3.1

[a]Reference [25] $\gamma = 75.8$.
[b]Reference [39] $\gamma = 56$,
[c]Reference [26] $\gamma = 105$.
[d]Reference [25] $\gamma = 87$.
[e]Reference [47] $\gamma = 73.7$.
[f]Reference [29] $\gamma = 69$ (single crystal).

as $N(E_F) = m^* k_F/\hbar^2\pi^2$, with m^* being the single isotropic effective mass m^*, and k_F the Fermi momentum. Assuming that the calculated density of states at E_F, $D(E_F)$, can likewise be related to a single effective DOS mass m_s, we obtain estimates of the mass enhancement over the calculated DOS mass m^*/m_s by comparing the measured $N(E_F)$ (obtained from γ) and the computed density of states at E_F, $D(E_F)$. While in reality, the density of states and effective masses are expected to be anisotropic, thermodynamic measurements, such as specific heat, are averages over FS; hence simple analyses as this may provide a reasonable estimate of m^*/m_s. We note that the calculated DOS mass m_s may not totally correspond to the band mass, usually referred to as m_b.

Table I summarizes results drawn from the various theoretical scenarios we have considered in this work. In particular, we show the calculated total DOS at the E_F, $D(E_F)$, and mass enhancement over the DOS mass m^*/m_s. For a given theoretical scenario, different values of estimated m^*/m_s for each skutterudite correspond to γ's obtained from specific heat measurements by different groups. The estimated mass enhancements m^*/m_s in the range of 2–4, give an indication of the correlation strength.

V. DISCUSSION

We have presented a comprehensive study of band structure, DOS, and FS for f-electron systems of type $R\mathrm{Pt_4Ge_{12}}$ (where R = La, Ce, Pr), using various theoretical scenarios such as PBE, PBE + SOC, and PBE + SOC + U within the two choices of treating the f electrons, as valence or core electrons. Our calculations show several bands crossing the E_F giving rise to multiple FS.

As expected, when the f electrons are treated as part of core, the three compounds show almost identical band structure, and thus similar FS, for a given theoretical scenario. Scenarios where SOC is present or absent, show different FS due to the fact that SOC lifts band degeneracy and shift bands, thus increasing the number of FS (especially at Γ point) and changing slightly the FS topology.

When the f electrons are treated in valence the three compounds show some slight differences. Although SOC has the same trends on the band structure as mentioned before, the increasing number of f electrons from 0 to 2 and the increase of correlations by adding the Hubbard parameter U on top of the PBE + SOC approximation, makes things more interesting. Our calculations within PBE + SOC approximation reveal the presence of six FS for the $\mathrm{LaPt_4Ge_{12}}$, four of them having a holelike character and the other two electronlike character. While increasing the number of f electrons, the hole pockets get filled and three of them disappear going from $\mathrm{LaPt_4Ge_{12}}$ to $\mathrm{PrPt_4Ge_{12}}$, while the electron pockets increase their surface. The effects of filling the hole pockets at Γ point are reversed with increasing correlations effects between the f electrons within the PBE + SOC + U approximation. Although these compounds have two electronlike and one holelike FS in common, independently of the theoretical scenario used, the hole pockets at Γ point are dependent on the theoretical scenario we used in our calculations. Thus, comparison of our theoretical predictions with de Hass–van Alphen [69–71] experiments for $\mathrm{LaPt_4Ge_{12}}$ and $\mathrm{PrPt_4Ge_{12}}$ [27] and new experiments for $\mathrm{CePt_4Ge_{12}}$ are desirable to validate the topology and the number of FS in $R\mathrm{Pt_4Ge_{12}}$ compounds.

While our theoretical calculations cannot directly explain superconductivity, they may have significance with respect to the multiband superconductivity or anisotropic nature of the pairing, as indicated by experiments on $\mathrm{PrPt_4Ge_{12}}$ and $\mathrm{LaPt_4Ge_{12}}$. Our calculations find a small amount of Pr − 4f states admixed with Ge-p states in $\mathrm{PrPt_4Ge_{12}}$, a feature obviously different from that in $\mathrm{LaPt_4Ge_{12}}$. This is confirmed by soft x-ray photoemission experiments on $\mathrm{PrPt_4Ge_{12}}$ [41,42] that show a finite contribution of Pr 4f to the states near E_F. Additionally, superconducting gaps are effected [19,47] by Ce substitution of Pr, i.e., $\mathrm{Pr_{1-x}Ce_xPt_4Ge_{12}}$, suggesting that the filler atoms may affect superconductivity. Based on these, it is conceivable that superconductivity is a consequence of Cooper pairs formed by the s, p, and d electrons of the Pt and Ge atoms in the $\mathrm{LaPt_4Ge_{12}}$, while superconductivity in the $\mathrm{PrPt_4Ge_{12}}$ is more unusual since in addition to s, p, and d electrons we also have f electrons at the E_F. As we have remarked earlier, since the $\mathrm{PrPt_4Ge_{12}}$ has anisotropic f character on the FS, while the $\mathrm{LaPt_4Ge_{12}}$ does not, this may lead to different electron-phonon couplings between various FS, and hence different forms of pairing. Agreement between theoretical and experimental critical temperatures for different lanthanum

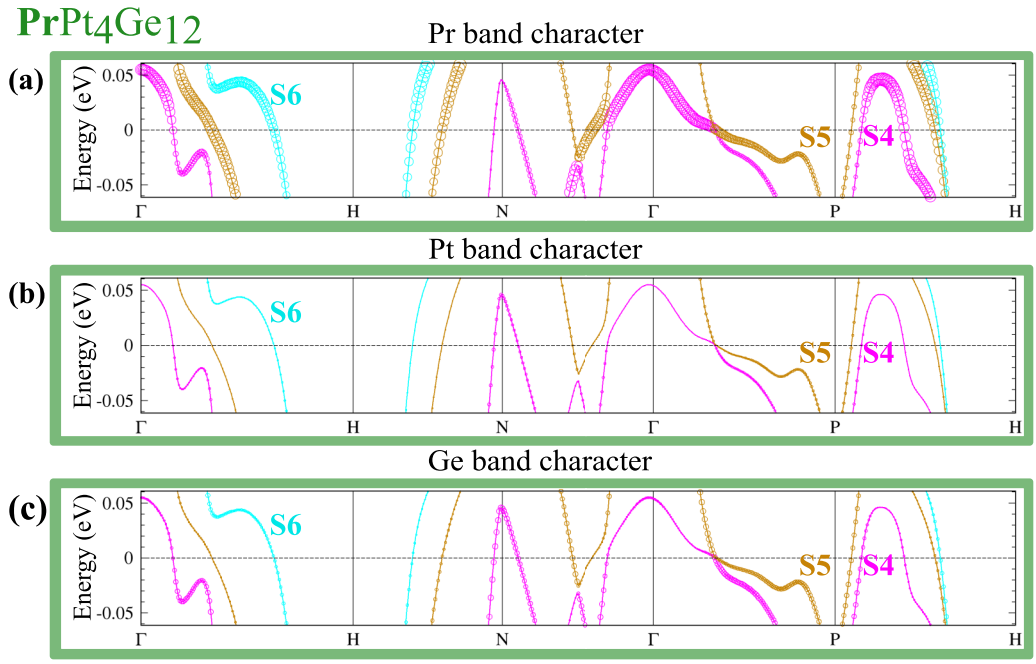

FIG. 9. Electronic band structure of $PrPt_4Ge_{12}$ showing the atomic character of the bands. This figure enlarges the energy range near the Fermi energy of the band structure previously shown in Fig. 4. The sizes of the open circles at a given energy and momentum represent the wave function amplitude corresponding to a given atom as labeled in each panel.

filled skutterudite [72] showed that these compounds are phonon-mediated superconductors. Thus, besides the average electron-phonon coupling in lanthanum filled skutterudite [72], it would be interesting to calculate electron-phonon couplings for each FS in other filled skutterudite compound.

We have shown that independent of the theoretical scenario used in our calculations (PBE, PBE + SOC, or PBE + SOC + U) the calculated total DOS has a pseudogap which could imply the tunability of these materials through a metal to insulator transition. This may be relevant in view of the sustained interest in the skutterudites as possible next generation thermoelectric materials. As discussed in Ref. [51], large Seebeck coefficient S (related to the thermopower figure of merit ZT) can be achieved by driving the system close to a metal to insulator transition. Specifically, close to the metal-insulator transition, the thermoelectric properties of the Sb substituted $LaPt_4Ge_{12-x}Sb_x$ compounds were found to be greatly enhanced compared to the undoped $LaPt_4Ge_{12}$ compound [51]. We suggest similar experiments on electron-doped $CePt_4Ge_{12}$ and $PrPt_4Ge_{12}$ compounds to test if the figure of merit is larger in these compounds compared to that on the stoichiometric compounds. We note that while DFT calculations are not able to treat the energy variation of mobility (and hence lifetime) that can modify results for Seebeck coefficient $S(T)$, a method such as DMFT, which is able to calculate finite-T lifetime, may provide further understanding of $S(T)$.

Finally, we mention that our results are consistent with previous DOS calculations [25,26] that comprise a limited set of results and a small subset of our more extensive work. However, our band structure and FS results differ substantially from those presented in a recent paper [28], which used the PBEsol approximation. We also performed calculations using the PBEsol approximation and found the results to be very similar to those obtained using the PBE approximation. Our results also reveal challenges confronted by DFT methods and its extension for correlated materials. We showed that the DFT + U method can only qualitatively explain the soft x-ray photoemission experiments on $PrPt_4Ge_{12}$. Thus, it would be desirable to use more advance methods for correlated materials, such as DFT + eDMFT, in order to explain quantitatively the experimental results.

ACKNOWLEDGMENTS

M.W. acknowledges support from the Department of Energy under Grant No. DE-SC0014506. K.F.Q. acknowledges a QuantEmX grant from ICAM and the Gordon and Betty Moore Foundation, Grant No. GBMF5305, which partly funded this work. G.L.P. and K.H. were supported by the U.S. Department of Energy, Office of Science, Basic Energy Sciences, as a part of the Computational Materials Science Program, funded by the U.S. Department of Energy, Office of Science, Basic Energy Sciences, Materials Sciences and Engineering Division. We thank Di Xiao, G. Malcolm Stocks, Gabriel Kotliar, and Carmen Almasan for useful discussions.

APPENDIX A: ELECTRONIC BAND STRUCTURE: f ELECTRONS IN CORE

In some systems, the states of f electrons behave as inert localized states, hybridizing very little or not at all with the other states in the system. To understand the effects of f-electron hybridization, we present the results of calculations when the f electrons are treated as core electrons. In Fig. 6 we show these calculations within the PBE and PBE + SOC approximations. We find that the electronic band structure

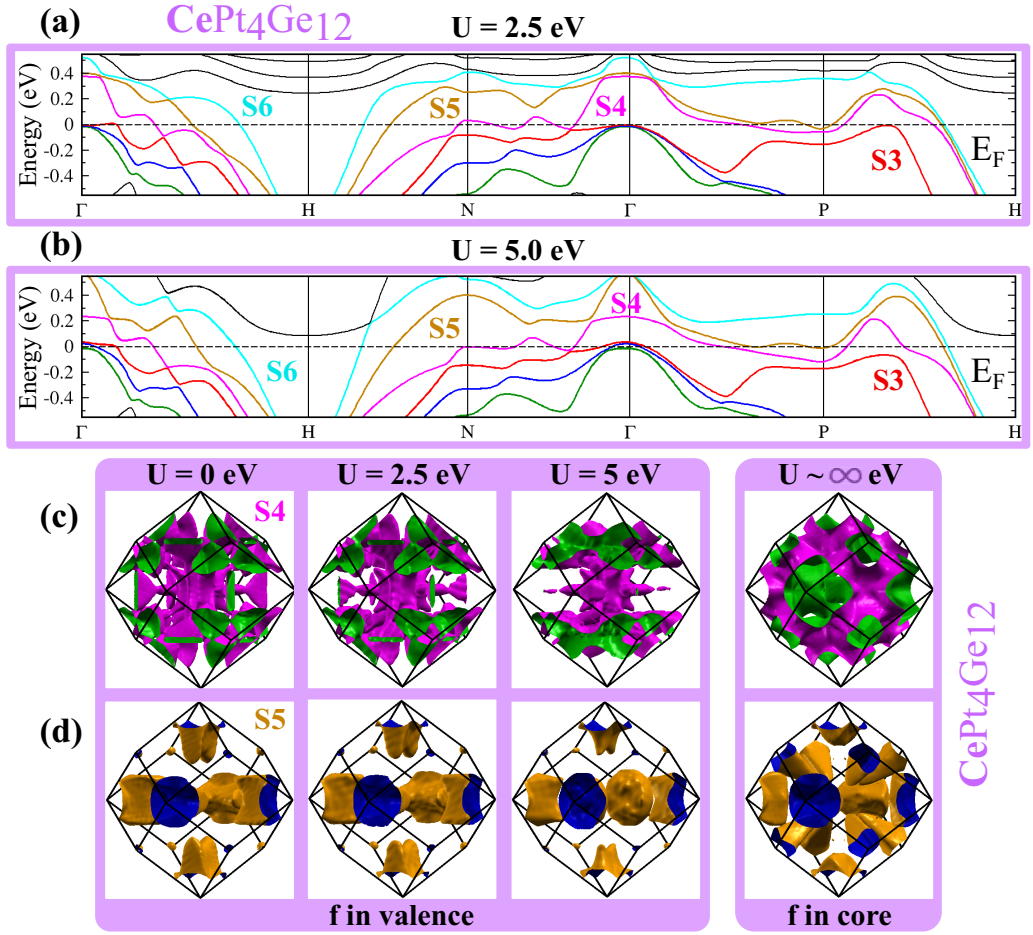

FIG. 10. Correlations effects on the electronic band structure and FS for $CePt_4Ge_{12}$. The results presented in this figure were obtained using the WIEN2K code with the PBE + SOC + U approximation treating the f electrons as valence electrons (exception are the results presented in the $U \sim \infty$ eV panel,which correspond to calculations using the PBE + SOC approximation treating the f electrons as core electrons). The electronic band structure plots shown here are on the same scale, plotted with the same color code for the lines representing the bands and with the same labels for the Fermi surfaces as in Fig. 4(d). (a) and (b) The electronic band structure for calculations with U of 2.5 and 5 eV. (c) and (d) The evolution with correlations for two distinct FS.

within a given approximation for the RPt_4Ge_{12} compounds is almost identical when the f electrons are treated as core. This implies that all the interesting low temperature properties of $CePt_4Ge_{12}$ and $PrPt_4Ge_{12}$ are mostly due to the f electrons states and their hybridization with the other states in the system.

APPENDIX B: FAT-BAND REPRESENTATION

By projecting the band wave function onto the atomic orbitals of a particular atom, we obtain the band structures shown by solid lines + open circles, where the size of the circles at an energy and momentum point are proportional to the absolute value of the wave-function amplitude corresponding to that given atom [62]. In these plots the size of the circle corresponds to the atomic character and is shown for one atom only, even though the band wave functions forming the bands have contributions from all the atoms (of the same type) within the unit cell.

In Fig. 7 we plot the electronic band structure with the atomic character for $LaPt_4Ge_{12}$. Looking at Figs. 7(a), 7(b) and 7(c) corresponding to the La, Pt, and Ge atomic character, we see that around the Fermi energy the electronic character comes mostly from the Ge and Pt atoms, consistent with the previously presented atom projected DOS in Fig. 2. At the same time, looking at the the first column in Fig. 3, we see that for Pt atoms the largest DOS at the E_F comes from p and d states and for the case of Ge the maximum DOS comes from p states. Thus, it may tempting to say that for $LaPt_4Ge_{12}$ compound the electrons involved in superconductivity would mostly be Ge p states plus some Pt p and d states. With reference to the notation in Fig. 4 for FS, here we can see that the S1, S2, and S6 FS are mostly Ge in character, while S3, S4, and S5 have contributions from both Ge and Pt ions. Notably, La is largely absent from the FS.

Figure 8 shows fat-band plots for $CePt_4Ge_{12}$. The discussion here follows that of Fig. 7 for $LaPt_4Ge_{12}$, with the additional fact that for $CePt_4Ge_{12}$ the FS have moderate f character in addition.

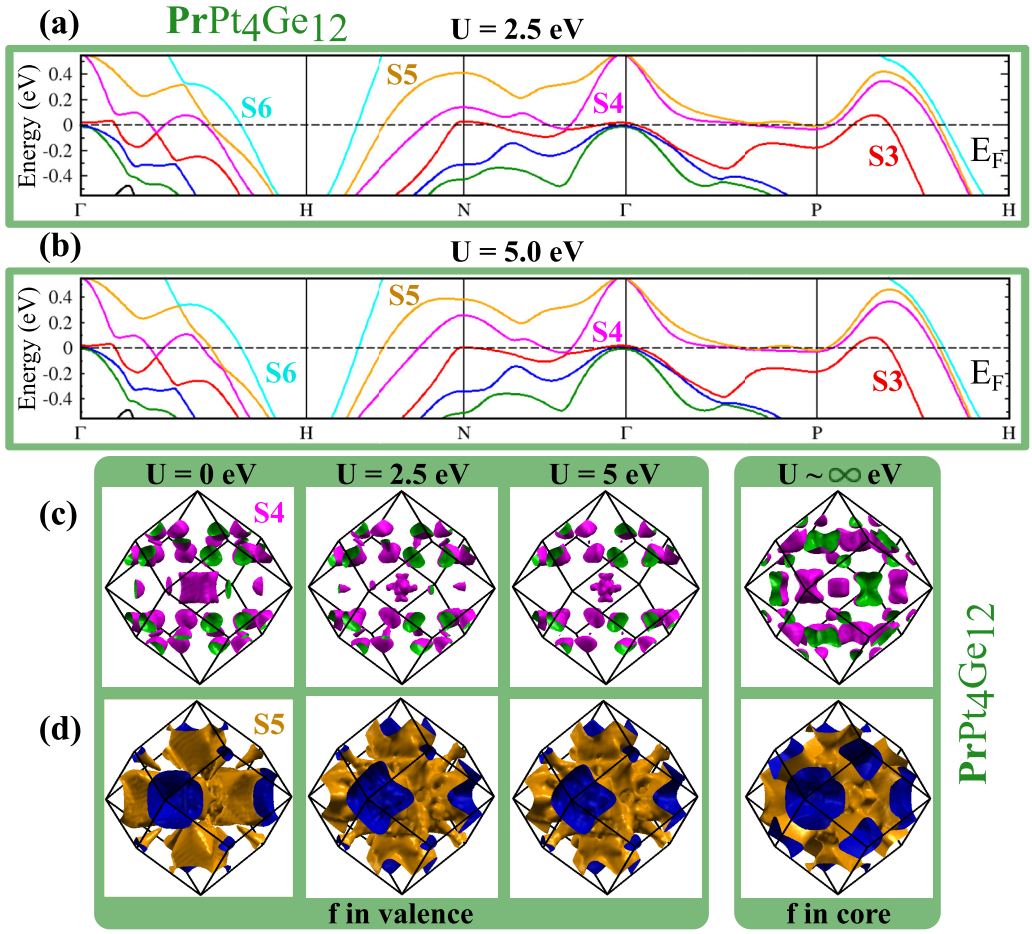

FIG. 11. Correlations effects on the electronic band structure and FS for $PrPt_4Ge_{12}$. The results presented in this figure were obtained using the WIEN2K code with the PBE + SOC + U approximation treating the f electrons as valence electrons (exception are the results presented in the $U \sim \infty$ eV panel, which correspond to calculations using the PBE + SO approximation treating the f electrons as core electrons). The electronic band structure plots shown here are on the same scale, plotted with the same color code for the lines representing the bands and with the same labels for the Fermi surfaces as in Fig. 4(f). (a) and (b) The electronic band structure for calculations with U of 2.5 and 5 eV. (c) and (d) The evolution with correlations for two distinct FS.

Likewise, in Fig. 9 we show fat-band plots for $PrPt_4Ge_{12}$. A similar discussion can be made as before for the case of $LaPt_4Ge_{12}$ and $CePt_4Ge_{12}$ with the additional fact that for $PrPt_4Ge_{12}$ the FS have strong f character. In addition, for the $PrPt_4Ge_{12}$ compound if we look at Fig. 9(a), where we show the Pr contribution to the FS, we see that the f character of the FS is anisotropic. For example, compare the strength (size of the circles) of Pr f character at the two intersections of the S4 band with the E_F between points P and N. In analogy with Pb, one could suggest that anisotropic band character could lead to anisotropic electron-phonon couplings for these FS. This makes for a strong case for calculating electron-phonon couplings in the $LaPt_4Ge_{12}$ and $PrPt_4Ge_{12}$ skutterudites, and exploring if f-electron coupling leads to multigap pairing in the case of $PrPt_4Ge_{12}$.

APPENDIX C: EFFECTS OF U ON BANDS AND FERMI SURFACES

From band structure plots, Figs. 10(a) and 10(b) and Figs. 11(a) and 11(b), it is obvious that the band corresponding to the S6 FS does not change much as we increase the correlation, thus this FS is quite robust which indicates that it is probably mostly s, p, and d in character. On the other hand, plotting the S4 and S5 FS versus U [see Figs. 10(c) and 10(d) and Figs. 11(c) and 11(d)], we find that S4 is the most affected, followed by S5. This suggests that the S4 and S5 FS have stronger f character than S6. To confirm the contribution of f states to the S4 and S5 FS for $U \geqslant 0$ eV, we have also computed the FS for the case where the f electrons are treated as core electrons (in this case the FS has no f contribution). These results are shown in Figs. 10(c) and 10(d), and Figs. 11(c) and 11(d), labeled as $U \sim \infty$ eV. The fact that the topology of the FS for $U \geqslant 0$ eV is different than that of $U \sim \infty$ eV, confirms once again the presence of f character in the FS of $CePt_4Ge_{12}$ and $PrPt_4Ge_{12}$. In addition, if we compare the bands in Fig. 4(d) ($U = 0$) for $CePt_4Ge_{12}$ with Fig. 10 ($U > 0$) we see for example, that with increasing U, band S3 falls below E_F along the path P–H, but rises above at Γ.

Comparing Fig. 4(f) ($U = 0$) for $PrPt_4Ge_{12}$ with Fig. 11 ($U > 0$), we see that S3 similarly rises above E_F at Γ, creating a new FS sheet. Thus, in both $CePt_4Ge_{12}$ and $PrPt_4Ge_{12}$ compounds, we find that depending on the strength of correlation

parameter U, the S1, S2, and S3 FS can be present or absent. As mentioned in the discussion section, de Haas–van Alphen measurements could sort out the puzzle of FS number and indirectly give information of the correlation strength in the $CePt_4Ge_{12}$ and $PrPt_4Ge_{12}$ compounds.

APPENDIX D: EXPERIMENTAL LATTICE PARAMETERS AND ATOMIC POSITIONS USED IN THE CALCULATIONS

The atomic positions and lattice parameters used in the calculations for the three compounds are from experiments and given in Tables II, III and IV.

TABLE II. $LaPt_4Ge_{12}$: Experimental lattice parameters $a = 8.6235(3)$ Å and atomic coordinates within the cubic Im-3 space group (No. 204) [2].

Atom	Site	$[x, y, z]$
La	2*a*	[0.00000, 0.00000, 0.50000]
Pt	8*c*	[0.25000, 0.25000, 0.25000]
Ge	24*g*	[0.00000, 0.15173(3), 0.35497(3)]

TABLE III. $CePt_4Ge_{12}$: Experimental lattice parameters $a = 8.6156(5)$ Å and atomic coordinates within the cubic Im-3 space group (No. 204) [2].

Atom	Site	$[x, y, z]$
Ce	2*a*	[0.00000, 0.00000, 0.50000]
Pt	8*c*	[0.25000, 0.25000, 0.25000]
Ge	24*g*	[0.00000, 0.15136(5), 0.35447(5)]

TABLE IV. $PrPt_4Ge_{12}$: Experimental lattice parameters $a = 8.6111(6)$ Å and atomic coordinates within the cubic Im-3 space group (No. 204) [2].

Atom	Site	$[x, y, z]$
Pr	2*a*	[0.00000, 0.00000, 0.50000]
Pt	8*c*	[0.25000, 0.25000, 0.25000]
Ge	24*g*	[0.00000, 0.15127(2), 0.35432(2)]

[1] W. Jeitschko and D. Braun, Acta Crystallogr. Sect. B **33**, 3401 (1977).

[2] R. Gumeniuk, H. Borrmann, A. Ormeci, H. Rosner,W. Schnelle, M. Nicklas, Y. Grin, and A. Leithe-Jasper, Z. Kristallogr. **225**, 531 (2010).

[3] M. B. Maple, Z. Henkie, R. E. Baumbach, T. A. Sayles, N. P. Butch, P.-C. Ho, T. Yanagisawa, W. M. Yuhasz, R. Wawryk, T. Cichorek *et al.*, J. Phys. Soc. Jpn. **77**, 7 (2008).

[4] Y. Aoki, T. Tayama, T. Sakakibara, K. Kuwahara, K. Iwasa, M. Kohgi, W. Higemoto, D. E. MacLaughlin, H. Sugawara, and H. Sato, J. Phys. Soc. Jpn. **76**, 051006 (2007).

[5] A. Maisuradze, M. Nicklas, R. Gumeniuk, C. Baines, W. Schnelle, H. Rosner, A. Leithe-Jasper, Y. Grin, and R. Khasanov, Phys. Rev. Lett. **103**, 147002 (2009).

[6] A. Maisuradze, W. Schnelle, R. Khasanov, R. Gumeniuk, M. Nicklas, H. Rosner, A. Leithe-Jasper, Y. Grin, A. Amato, and P. Thalmeier, Phys. Rev. B **82**, 024524 (2010).

[7] N. Takeda and M. Ishikawa, J. Phys. Soc. Jpn. **69**, 868 (2000).

[8] A. Yamamoto, S. Wada, I. Shirotani, and C. Sekine, J. Phys. Soc. Jpn. **75**, 063703 (2006).

[9] C. Sekine, T. Uchiumi, I. Shirotani, and T. Yagi, Phys. Rev. Lett. **79**, 3218 (1997).

[10] M. Yoshizawa, Y. Nakanishi, M. Oikawa, C. Sekine, I. Shirotani, S. R. Saha, H. Sugawara, and H. Sato, J. Phys. Soc. Jpn. **74**, 2141 (2005).

[11] B. Yan, L. Müchler, X.-L. Qi, S.-C. Zhang, and C. Felser, Phys. Rev. B **85**, 165125 (2012).

[12] J. C. Smith, S. Banerjee, V. Pardo, and W. E. Pickett, Phys. Rev. Lett. **106**, 056401 (2011).

[13] T. Masatoshi, S. Hitoshi, M. Ko-ichi, S. Takahito, K. Kuniyuki, A. Yuji, and S. Hideyuki, J. Phys. Soc. Jpn. **77**, 124702 (2008).

[14] E. D. Bauer, N. A. Frederick, P.-C. Ho, V. S. Zapf, and M. B. Maple, Phys. Rev. B **65**, 100506(R) (2002).

[15] M. B. Maple, P.-C. Ho, V. S. Zapf, N. A. Frederick, E. D. Bauer, W. M. Yuhasz, F. M. Woodward, and J. W. Lynn, J. Phys. Soc. Jpn. **71**, 23 (2002).

[16] M. Maple, N. Frederick, P.-C. Ho, W. Yuhasz, T. Sayles, N. Butch, J. Jeffries, and B. Taylor, Physica B: Condensed Matter **359-361**, 830 (2005).

[17] M. Maple, Z. Henkie, W. Yuhasz, P.-C. Ho, T. Yanagisawa, T. Sayles, N. Butch, J. Jeffries, and A. Pietraszko, J. Magn. Magn. Mater. **310**, 182 (2007).

[18] H. Sato, Y. Aoki, D. Kikuchi, H. Sugawara, W. Higemoto, K. Ohishi, T. Ito, R. Heffner, S. Saha, A. Koda *et al.*, Physica B (Amsterdam) **404**, 749 (2009).

[19] I. Jeon, K. Huang, D. Yazici, N. Kanchanavatee, B. D. White, P.-C. Ho, S. Jang, N. Pouse, and M. B. Maple, Phys. Rev. B **93**, 104507 (2016).

[20] W. M. Yuhasz, N. P. Butch, T. A. Sayles, P.-C. Ho, J. R. Jeffries, T. Yanagisawa, N. A. Frederick, M. B. Maple, Z. Henkie, A. Pietraszko *et al.*, Phys. Rev. B **73**, 144409 (2006).

[21] D. T. Morelli and G. P. Meisner, J. Appl. Phys. **77**, 3777 (1995).

[22] B. C. Sales, D. Mandrus, B. C. Chakoumakos, V. Keppens, and J. R. Thompson, Phys. Rev. B **56**, 15081 (1997).

[23] G. S. Nolas, J. L. Cohn, and G. A. Slack, Phys. Rev. B **58**, 164 (1998).

[24] B. C. Sales, D. Mandrus, and R. K. Williams, Science **272**, 1325 (1996).

[25] R. Gumeniuk, W. Schnelle, H. Rosner, M. Nicklas, A. Leithe-Jasper, and Y. Grin, Phys. Rev. Lett. **100**, 017002 (2008).

[26] R. Gumeniuk, K. O. Kvashnina, W. Schnelle, M. Nicklas, H. Borrmann, H. Rosner, Y. Skourski, A. A. Tsirlin, A. Leithe-Jasper, and Y. Grin, J. Phys.: Condens. Matter **23**, 465601 (2011).

[27] B. Bergk, J. Klotz, T. Förster, R. Gumeniuk, A. Leithe-Jasper, V. Lorenz, W. Schnelle, M. Nicklas, H. Rosner, Y. Grin *et al.*, Phys. Rev. B **99**, 245115 (2019).

[28] L. S. S. Chandra, M. K. Chattopadhyay, S. B. Roy, and S. K. Pandey, Philos. Mag. **96**, 2161 (2016).

[29] J. L. Zhang, Y. Chen, L. Jiao, R. Gumeniuk, M. Nicklas, Y. H. Chen, L. Yang, B. H. Fu, W. Schnelle, H. Rosner *et al.*, Phys. Rev. B **87**, 064502 (2013).

[30] L. Peters, I. Di Marco, P. Thunström, M. I. Katsnelson, A. Kirilyuk, and O. Eriksson, Phys. Rev. B **89**, 205109 (2014).

[31] L. Petit, Z. Szotek, M. Lüders, and A. Svane, J. Phys.: Condens. Matter **28**, 223001 (2016).

[32] X. X. Xi, Rep. Prog. Phys. **71**, 116501 (2008).

[33] J. Kortus, I. I. Mazin, K. D. Belashchenko, V. P. Antropov, and L. L. Boyer, Phys. Rev. Lett. **86**, 4656 (2001).

[34] A. Floris, A. Sanna, S. Massidda, and E. K. U. Gross, Phys. Rev. B **75**, 054508 (2007).

[35] B. L. Blackford and R. H. March, Phys. Rev. **186**, 397 (1969).

[36] E. Bauer, A. Grytsiv, X.-Q. Chen, N. Melnychenko-Koblyuk, G. Hilscher, H. Kaldarar, H. Michor, E. Royanian, G. Giester, M. Rotter *et al.*, Phys. Rev. Lett. **99**, 217001 (2007).

[37] H. Rosner, J. Gegner, D. Regesch, W. Schnelle, R. Gumeniuk, A. Leithe-Jasper, H. Fujiwara, T. Haupricht, T. C. Koethe, H.-H. Hsieh *et al.*, Phys. Rev. B **80**, 075114 (2009).

[38] R. Gumeniuk, M. Schöneich, A. Leithe-Jasper, W. Schnelle, M. Nicklas, H. Rosner, A. Ormeci, U. Burkhardt, M. Schmidt, U. Schwarz *et al.*, New J. Phys. **12**, 103035 (2010).

[39] H. Pfau, M. Nicklas, U. Stockert, R. Gumeniuk, W. Schnelle, A. Leithe-Jasper, Y. Grin, and F. Steglich, Phys. Rev. B **94**, 054523 (2016).

[40] L. S. Chandra, M. Chattopadhyay, and S. Roy, Philos. Mag. **92**, 3866 (2012).

[41] Y. Nakamura, H. Okazaki, R. Yoshida, T. Wakita, M. Hirai, Y. Muraoka, H. Takeya, K. Hirata, H. Kumigashira, M. Oshima *et al.*, J. Phys. Soc. Jpn. **79**, 124701 (2010).

[42] Y. Nakamura, H. Okazaki, R. Yoshida, T. Wakita, H. Takeya, K. Hirata, M. Hirai, Y. Muraoka, and T. Yokoya, Phys. Rev. B **86**, 014521 (2012).

[43] A. Gurevich, Physica C: Superconductivity **456**, 160 (2007).

[44] S. Tsuda, T. Yokoya, S. Shin, Y. Takano, H. Kito, A. Matsushita, F. Yin, J. Itoh, and H. Harima, Physica C **412-414**, 36 (2004).

[45] S. Tsuda, T. Yokoya, and S. Shin, Physica C: Superconductivity **456**, 126 (2007).

[46] G. I. Lykken, A. L. Geiger, K. S. Dy, and E. N. Mitchell, Phys. Rev. B **4**, 1523 (1971).

[47] Y. P. Singh, R. B. Adhikari, S. Zhang, K. Huang, D. Yazici, I. Jeon, M. B. Maple, M. Dzero, and C. C. Almasan, Phys. Rev. B **94**, 144502 (2016).

[48] K. Huang, L. Shu, I. K. Lum, B. D. White, M. Janoschek, D. Yazici, J. J. Hamlin, D. A. Zocco, P.-C. Ho, R. E. Baumbach *et al.*, Phys. Rev. B **89**, 035145 (2014).

[49] F. Kanetake, H. Mukuda, Y. Kitaoka, K. ichi Magishi, H. Sugawara, K. M. Itoh, and E. E. Haller, J. Phys. Soc. Jpn. **79**, 063702 (2010).

[50] M. Nicklas, S. Kirchner, R. Borth, R. Gumeniuk, W. Schnelle, H. Rosner, H. Borrmann, A. Leithe-Jasper, Y. Grin, and F. Steglich, Phys. Rev. Lett. **109**, 236405 (2012).

[51] S. Humer, E. Royanian, H. Michor, E. Bauer, A. Grytsiv, M. X. Chen, R. Podloucky, and P. Rogl, From superconductivity towards thermoelectricity: Ge-based skutterudites, in *New Materials for Thermoelectric Applications: Theory and Experiment*, edited by V. Zlatic and A. Hewson, NATO Science for Peace and Security Series B: Physics and Biophysics (Springer, Dordrecht, 2013).

[52] G. A. Slack, *CRC Handbook of Thermoelectrics* (CRC, Boca Raton, FL, 1995).

[53] M. Beekman, D. T. Morelli, and G. S. Nolas, Nat. Mater. **14**, 1182 (2015).

[54] G. A. Slack and V. G. Tsoukala, J. Appl. Phys. **76**, 1665 (1994).

[55] P. Hohenberg and W. Kohn, Phys. Rev. **136**, B864 (1964).

[56] W. Kohn and L. J. Sham, Phys. Rev. **140**, A1133 (1965).

[57] J. P. Perdew, K. Burke, and M. Ernzerhof, Phys. Rev. Lett. **77**, 3865 (1996).

[58] G. Kresse and J. Furthmuller, Phys. Rev. B **54**, 11169 (1996).

[59] G. Kresse and D. Joubert, Phys. Rev. B **59**, 1758 (1999).

[60] P. Blaha, K. Schwarz, G. K. H. Madsen, D. Kvasnicka, J. Luitz, R. Laskowski, F. Tran, and L. D. Marks, *WIEN2k, An Augmented Plane Wave + Local Orbitals Program for Calculating Crystal Properties* (Karlheinz Schwarz, Techn. Universität Wien, Austria, 2018).

[61] W. Setyawan and S. Curtarolo, Comput. Mater. Sci. **49**, 299 (2010).

[62] K. Schwarz, P. Blaha, and S. Trickey, Mol. Phys. **108**, 3147 (2010).

[63] S. L. Dudarev, G. A. Botton, S. Y. Savrasov, C. J. Humphreys, and A. P. Sutton, Phys. Rev. B **57**, 1505 (1998).

[64] V. I. Anisimov, I. V. Solovyev, M. A. Korotin, M. T. Czyżyk, and G. A. Sawatzky, Phys. Rev. B **48**, 16929 (1993).

[65] K. Haule, C.-H. Yee, and K. Kim, Phys. Rev. B **81**, 195107 (2010).

[66] K. Haule, J. Phys. Soc. Jpn. **87**, 041005 (2018).

[67] DFT + Embedded DMFT functional, http://hauleweb.rutgers.edu/tutorials/, see Ref. [61].

[68] C. Kittel, *Introduction to Solid State Physics*, 8th ed. (Wiley, New York, 2005).

[69] P. Rourke and S. Julian, Comput. Phys. Commun. **183**, 324 (2012).

[70] S. F. Blake, M. D. Watson, A. McCollam, S. Kasahara, R. D. Johnson, A. Narayanan, G. L. Pascut, K. Haule, V. Kiryukhin, T. Yamashita *et al.*, Phys. Rev. B **91**, 121105(R) (2015).

[71] M. Brasse, L. Chioncel, J. Kuneš, A. Bauer, A. Regnat, C. G. F. Blum, S. Wurmehl, C. Pfleiderer, M. A. Wilde, and D. Grundler, Phys. Rev. B **88**, 155138 (2013).

[72] H. M. Tütüncü, E. Karaca, and G. P. Srivastava, Phys. Rev. B **95**, 214514 (2017).